JMEPEG (2006) 15:581-590
DOI: 10.1361/105994906X136034
©ASM International
1059-9495/$19.00

Microstructure, Microchemistry, and Prediction of Long-Term Diffusion Behavior of Chloride in Concrete

T. Karthikeyan, Arup Dasgupta, P. Magudapathy, S. Saroja, M. Vijayalakshmi, K.G.M. Nair, K.P.N. Murthy, and Baldev Raj

(Submitted July 11, 2005; in revised form January 17, 2006)

Microstructural and microchemical features of two types of concrete are investigated employing electron and ion optical techniques. The first type is the concrete cured in seawater or normal water. The second type is concrete cured in normal water and exposed subsequently to seawater. Major constituent phases of concrete and differences in their distribution due to different curing media are identified. Chloride profiles in different concretes are evaluated using the proton induced x-ray emission technique. Diffusion coefficient *D* was calculated by modeling the diffusion process and comparing with measured profiles. *D*, thus estimated, is found to be ~1.8×10^{-9} m^2/s, which is higher than the reported values of ~10^{-11} to 10^{-13} m^2/s. The faster diffusion of chloride in seawater-cured concrete can be attributed to the availability of water medium in wet concrete, in the initial stages of the hydration of cement. The prediction of the concentration profile of chloride in a layer of 100 mm of 28% fly ash containing concrete over concrete exposed to seawater is carried out. For the worst scenario, analytical estimates of the concentration of chloride as a function of time at a distance of 100 mm in the fly ash containing concrete were made. The concentration profiles of chloride expected after 40 years in the fly ash-containing concrete were also estimated using diffusion coefficient values available in the literature.

Keywords chloride diffusion, concrete, microstructure, proton-induced x-ray emission (PIXE)

1. Introduction

Two physicochemical processes limit the useful life of reinforced concrete, namely, carbonation and chlorination. Under normal circumstances, the steel bars in concrete are protected from corrosion by the high alkalinity (pH ~ 13) of the cement phase. However, some of the chemical reactions, like that of $Ca(OH)_2$ with CO_2, reduce the pH in the water in the surrounding pores in the concrete around the steel bars. This process is called *carbonation*. This reduction in pH is harmful to the formation of passive ferric oxide film ($\gamma FeOOH$) over the steel bars that reinforce the concrete. A similar effect is also produced by the presence of chloride ions, from sources like $CaCl_2$, a main component used to harden the concrete, the use of either seawater or beach aggregates to mix concrete, the chlorides in the deicing salts in cold countries, and the absorption/ingression of chloride from either sea or air in coastal areas. Complete breakdown of the passive film occurs when the ratio of the concentration of chloride to hydroxide exceeds 0.6, leading to depassivation of the steel bars. Chlorination of the concrete is also deleterious to its mechanical behavior. Hence, the acceptable level of chloride in concrete is specified to be as low as 0.05 wt.% (Ref 1).

The chlorination of concrete has been studied employing a wide range of techniques like potentiometric titration (Ref 2), electrical migration (Ref 3), radionuclide diffusion (Ref 4), electron and ion optical methods like electron probe microanalysis (Ref 5), proton-induced x-ray emission (PIXE) (Ref 6), and modeling (Ref 7-10). These studies have shown that the transport of chloride ions in concrete proceeds via the aqueous phase of the pore system. The dependence of chloride diffusion on the pore system and the water-to-cement ratio has also been studied (Ref 10). Many physicochemical processes occur during the transport of chloride ions through concrete; the reaction products get adsorbed, bound, or desorbed in the solid phases of the cement. It has been possible to show that all these processes are confined to a small distance from an imaginary "chlorination front." Simple analytical models (Ref 1, 7, 8), their modifications for different physicochemical processes and environmental conditions, and numerical methods (Ref 9, 11) have been developed for predicting the long-term behavior of concrete.

This article presents the microstructural variations that take place in concrete that is either cured in seawater or is exposed to seawater after curing. The diffusion coefficient of chloride in concrete cured in seawater has been evaluated using the chloride profiles measured using PIXE and modeling. The long-term consequence of chloride diffusion into concrete through an intermediate layer of 100 mm of concrete with 28% fly ash from a layer beneath that was exposed to seawater has been estimated using diffusion models.

2. Experimental

Samples were prepared from three types of concrete blocks:

- Sample 1: a concrete block (150 mm cube) cured for 70 days in normal water with a chloride content of ~20 ppm (<0.05 wt.%).
- Sample 2: a concrete block (150 mm cube) mixed and

T. Karthikeyan, Arup Dasgupta, P. Magudapathy, S. Saroja, M. Vijayalakshmi, K.G.M. Nair, K.P.N. Murthy, and **Baldev Raj**, Indira Gandhi Center for Atomic Research, Kalpakkam 603 102, India. Contact e-mail: saroja@igcar.ernet.in.

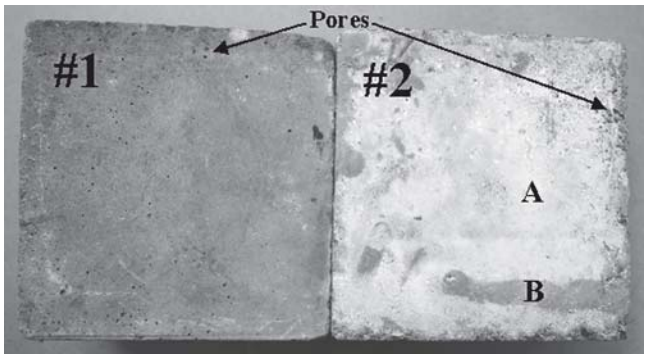

Fig. 1 Photographs of sample 1 (cured for 70 days in normal water) and sample 2 (cured in seawater)

poured with normal water but cured in seawater for 20 days.

- Sample 3: a block of well-cured (in normal water) concrete exposed to seawater for 7 days. The steel enforcement was at a distance of 280 mm from the surface of this block.

Microstructural and microchemical analyses were carried out using specimens taken from appropriate locations from the above three sample blocks. Two small sections (~25 × 25 mm) from the center and surface of sample 1 were mounted for analysis. For samples 2 and 3, specimens were taken from locations close to the surface, center (75 and 280 mm, respectively), and three equally spaced intermediate distances. The specimens were mounted, ground to obtain a flat surface, and coated with gold to obtain a conducting surface. The cleaning of debris after polishing was carried out in alcohol.

The mounted specimens were examined in a Philips XL 30 (Amsterdam, The Netherlands) environmental scanning electron microscope with an energy-dispersive analyzer for x-rays at an operating voltage of 30 keV. Secondary electron, backscattered electron, and x-ray images were obtained from appropriate regions. The PIXE analysis was carried out using an incident proton beam in a 1.7 MeV Tandetron (IGCAR, Kalpakkam) accelerator, collimated to a beam of 2 mm diameter to irradiate the sample. A 2 MeV beam energy and a 10 to 15 nA current were maintained during the experiment. The range of protons in concrete is expected to be of the order of 40 μm. An Si-Li detector with an active area of 30 mm^2, the energy resolution of which is 130 eV for Mn-Kα, was placed at an angle of 45° with respect to the beam direction for the PIXE measurements. The characteristic x-rays from the sample pass through a 50 μm Mylar window and traverse about 9 cm before entering into the Si(Li) detector.

3. Results

3.1 Visual Examination

Photographs of sample 1 (reference) and sample 2 (cured in seawater) are shown in Fig. 1. A comparison of the surfaces of the two samples shows no visible difference in the size and number of pores. However, distinct differences in their roughness and coloration were observed. Sample 1 had a smooth surface and was greenish-gray in appearance, while sample 2 had a rough surface, was white in appearance (region A) and possessed elongated features that were light yellow in appearance (region B).

3.2 Microstructural and Microchemical Analysis of the Two Types of Concrete

3.2.1 Comparison of Surface Structures. The microstructure and chemical composition from the surface of samples 1 (reference) and 2 were compared. The microstructures are shown in Fig. 2(a-c). The reference sample shows a structure predominantly of hydrated cement paste, interspersed with aggregate, which is a typical structure of concrete (Ref 12). The microstructures from region A and B of sample 2, shown in Fig. 2(b) and (c), respectively, exhibited different features. The surface was relatively rough and porous. A comparison of the chemical composition is made in Fig. 3. The energy-dispersive spectroscopy (EDS) spectrum from the reference sample shows the presence of Ca, Al, Fe, and Si, which is typical of a spectrum of cement. The O peak is not observed because elements with atomic number 11 and above can only be detected using a Be window. A marked difference between the spectra from samples 1 and 2 was the high levels of Mg observed in sample 2.

The presence of chloride on the surface of sample 2 is also observed. Further investigations on region B, shown in Fig. 2(c) revealed the presence of two distinct regions. The micrographs from the two regions are given in Fig. 4(a) and (b), corresponding to the porous regions (C) and the darker regions (D) in Fig. 2(c), respectively. The EDS spectra from the two regions are shown in Fig. 4(c) and (d). Figure 4(a) showed the presence of crystalline-faceted regions that were found to be rich in Ca (Fig. 4c), while Fig. 4(b) showed the presence of a needle-like structure with high levels of Mg (Fig. 4d). The presence of a significant amount of Mg on the surface of sample 2 is attributed to deposition of Mg salts from the seawater.

3.2.2 Comparison of Internal Structures. The microstructure of specimens taken from inner locations of the concrete blocks were studied, and no difference between the reference concrete and the seawater-cured concrete was observed. Figure 5(a) shows a typical low-magnification back scattered electron (BSE) image of a flat-ground surface of sample 2. The intensity of the BSE signal is mainly a function of the average atomic number of the local area of the sample (Ref 13), and the resultant contrast in the BSE image, combined with the EDS analysis, was used to identify the various features. A large piece of gravel aggregate is seen on the left side of the micrograph. Similarly, several sand aggregates are seen interspersed within the cement paste, at the other side. Aggregates are usually oxide minerals of Si and have a lower average Z value compared with the Ca-rich hydrated cement paste and, thus, exhibit a darker contrast. The very bright patches within the aggregate are, however, due to minerals with a higher Fe content. A finely intermixed structure of different gray-level contrasts is observed in the hydrated cement region due to the presence of various constituents. The hydration products have a lower average Z compared with unreacted cement due to the intake of water during hydration. Among the hydration products, $Ca(OH)_2$ has a higher Z compared with other hydration products, such as C-S-H (calcium silicate hydrate), ettringite (calcium aluminum trisulfate), which subsequently decomposes to calcium aluminum monosulfate (AFm). No evidence for the presence of bright and granular partially reacted cement grain was observed. The observed variations in contrast in the hydrated cement paste is, therefore, a result of the mixture of two primary cement phases, namely, C-S-H, which has a low

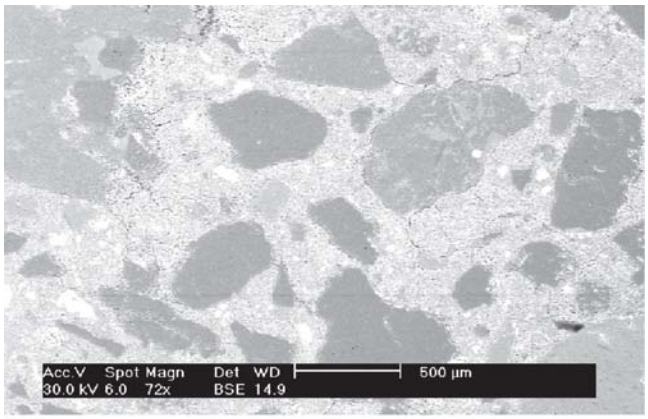

(a)

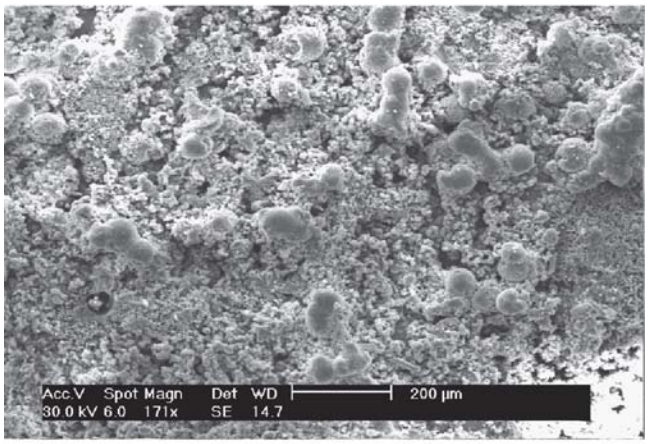

(b)

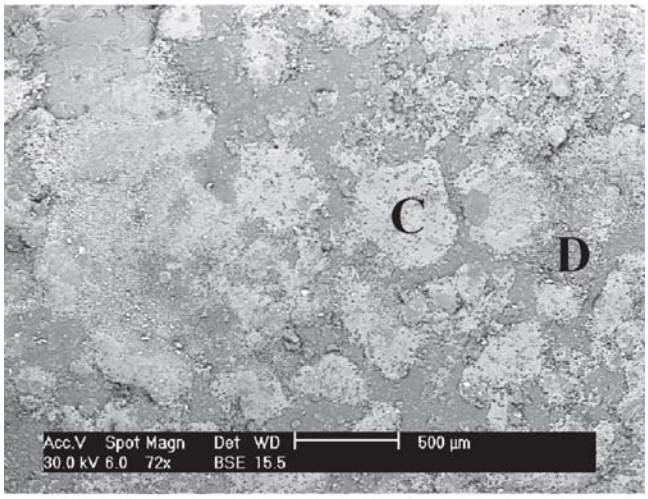

(c)

Fig. 2 SEM images of the surface of the samples: (a) reference sample showing regions predominantly containing cement; (b) surface of the seawater-cured sample showing porous structures from the regions, marked "A" in Fig. 1; and (c) seawater-cured sample from the region marked "B" in Fig. 1

contrast compared with the bright $Ca(OH_2)$. The third major phase in the cement (i.e., calcium aluminum sulfate hydrates, either metastable ettringite or stable AFm), have similar Z values as C-S-H and could not be distinguished in the BSE image even at high magnifications. Another important feature in Fig.

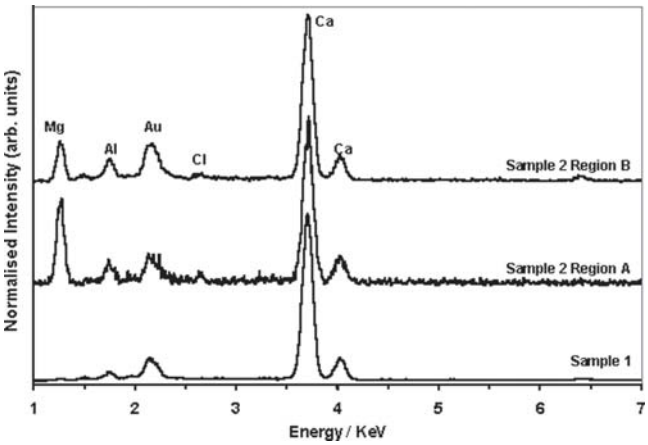

Fig. 3 Comparison of EDS spectra from the surface of concrete cured in seawater (sample 2) and reference concrete cured in normal water (sample 1) (ignore the Au peak). Both regions A and B of sample 2 contain more Cl and Mg than sample 1

5(a) is the interfacial transition (IFT) zone, corresponding to the interface between the aggregates (particularly large) and the hydrated cement paste (Ref 12). The IFT zone observed in Fig. 5(a) exhibited typical characteristics, such as relatively large $Ca(OH)_2$ crystals and other hydration products, within a large porous framework, resulting in an overall darker contrast. This is a result of the higher water-to-cement content ratio present adjacent to such large aggregates.

Cement constituent phases of C-S-H, $Ca(OH)_2$, and ettringite exhibit distinct morphologies, which could not be resolved in the ground specimen. Hence, scanning electron microscopy (SEM) analysis was carried out on a specimen from the as-fractured concrete surface. Figure 5(b) shows the high-magnification SEM image of hydrated cement paste. The long slender ettringite needles, the fine layered network morphology of C-S-H, and the hexagonal $Ca(OH)_2$ crystal could all be observed, along with the interspersed capillary pores. The structure of concrete can, therefore, be summarized as a heterogeneous mixture of gravel and sand aggregates, hydrated cement paste, consisting of CSH, ettringite, and calcium hydroxide, with an IFT zone and pore system.

The EDS spectra taken from several regions in the cement mass and aggregates showed the presence of Si, Ca, Al, Fe, S, and Cl in the sample. An attempt to distinguish between the hydration products based on EDS spectra was difficult. Because it was observed that chloride was confined to the cement regions, the analysis of the chloride content was restricted to the cement constituent. Although the SEM/EDS technique is not suitable for the accurate estimation of the chloride concentration from bulk regions, it has been used as a first approximation to arrive at a qualitative identification of the microchemistry. Furthermore, EDS is unsuitable for elemental quantification when the elements present are on the order of a few hundred parts per million. Hence, a detailed analysis has been carried out by PIXE, which will be discussed later.

3.3 Effect of Exposure of Seawater on Well-Cured Concrete

A cylindrical block of concrete, designated as sample 3, was well-cured in normal water and then exposed to seawater for about 7 days. Specimens, at intervals of ~70 mm from the

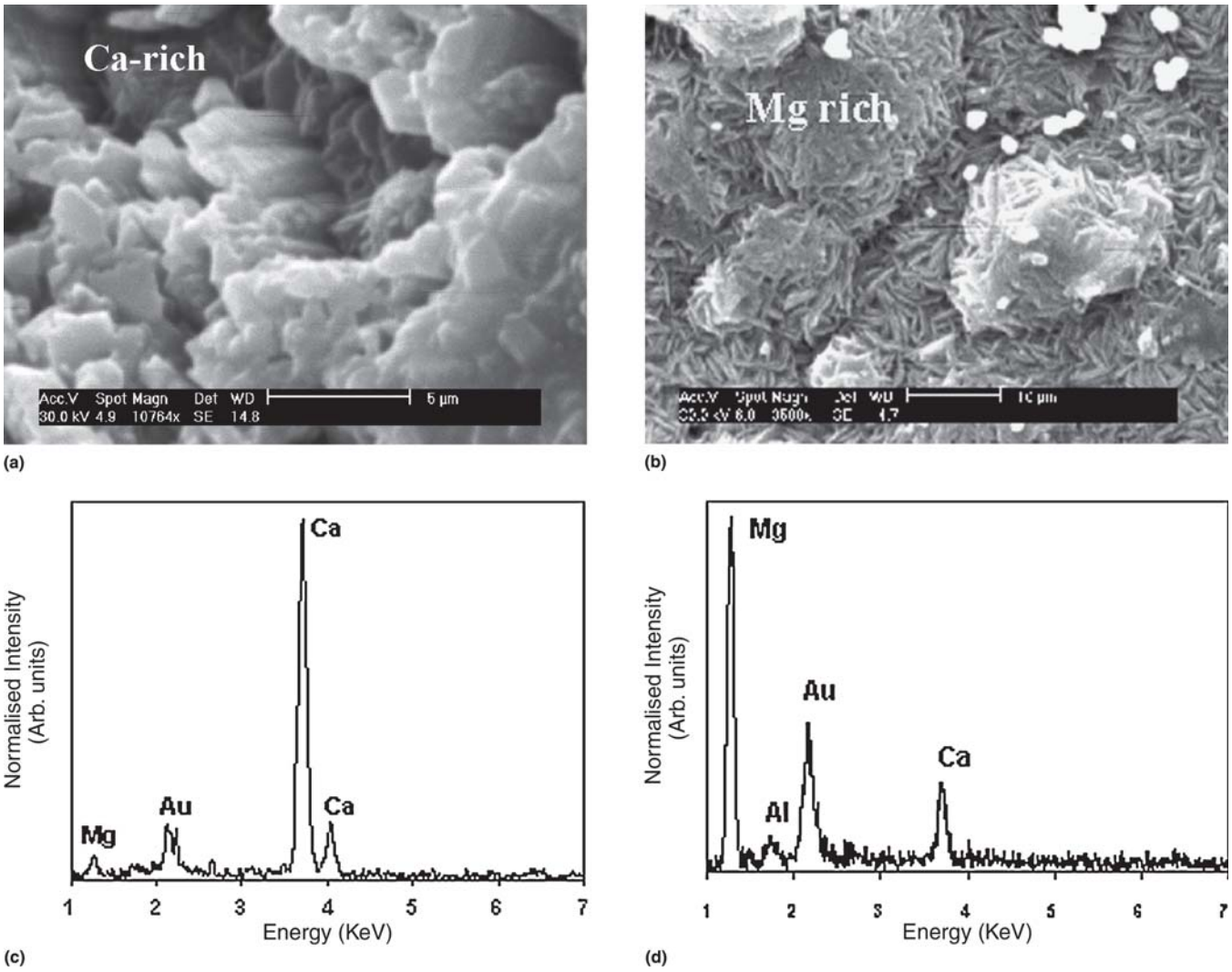

Fig. 4 (a) Faceted crystalline phase, which is Ca-rich. (b) Needle-like structure rich in Mg. (c) EDS spectra from the region in Fig. 4(a) and marked "C" in Fig. 2(a). (d) EDS spectra from the region shown in Fig. 4(b) and marked "D" in Fig. 2(a)

surface, were examined. At a distance of about 280 mm, the steel reinforcement was encountered. The concrete adhering to the steel was examined to determine the level of chloride and to assess the effect of chloride content in concrete on the corrosion characteristics of steel. The microstructure and EDS spectrum from a piece of concrete in contact with the steel is given in Fig. 6. The specimen did not include sand or aggregates.

The SEM image showed a microstructure that is typical of cement mass. The EDS spectrum did not show the presence of Fe or detectable levels of chloride. Hence, it can be concluded that the exposure of the surface of well-cured concrete to seawater for 7 days did not produce any change in the steel present at a distance of about 280 mm from the exposed surface or of the concrete in contact with the steel.

3.4 Estimation of Chloride Content

The estimation of low concentrations of chloride (i.e., a few hundred to a few thousand parts per million) is nearly at the detection limit of the EDS system. Resolving the chloride peak was difficult due to the low peak-to-background ratio. This precluded a reasonable quantification of the amount of chloride. Yet, the technique could be used to follow the relative change in concentration, because an observable change in the net intensity of the chloride peak was obtained between different samples. Proton-induced x-ray emission, a technique that is more appropriate for quantifying low concentrations of chloride, has been used for this purpose. It produces a low background due to the reduction in Bremsstrahlung radiation.

The chloride content in sample 1 was very low and was uniform across the thickness of the block. Comparison of EDS spectra from the surface and center of sample 2 (Fig. 7) showed an observable variation in the intensity of the chloride peak. The intensity at a depth of 75 mm from the surface (i.e., the center of the seawater-cured block) was comparable to the reference sample and was much lower than that at the surface.

The same specimen was analyzed by PIXE to obtain the variation of chloride as a function of distance from the surface. The spectra are shown in Fig. 8. The net intensity of chloride at the surface is higher than at distances further away from the surface or at the center of the 150 mm thick block. Such behavior is observed until a distance of about 35 to 40 mm. This suggests that the chloride content at the surface and up to a

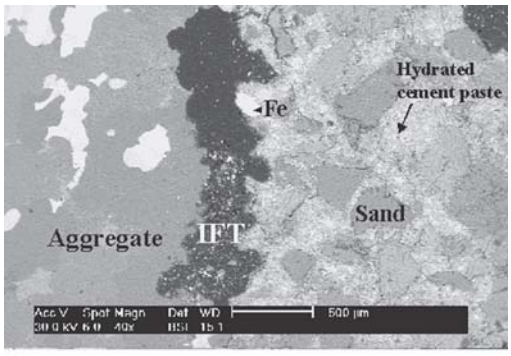

(a)

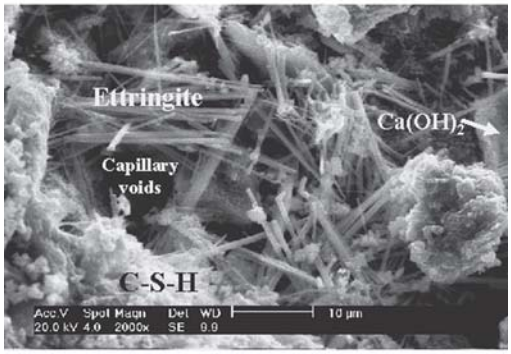

(b)

Fig. 5 (a) Microstructure across a cross section of a concrete block cured in seawater showing sand, cement, and minerals typical of an internal structure of concrete. (b) Magnified view of a fractured surface showing the various constituents in hydrated cement paste

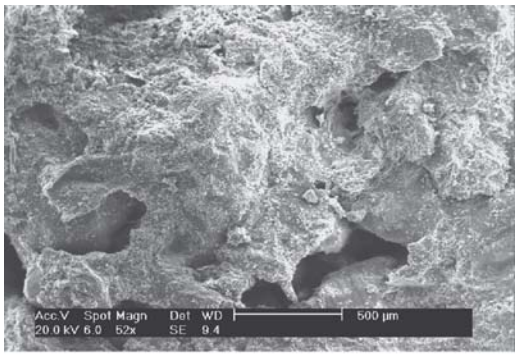

(a)

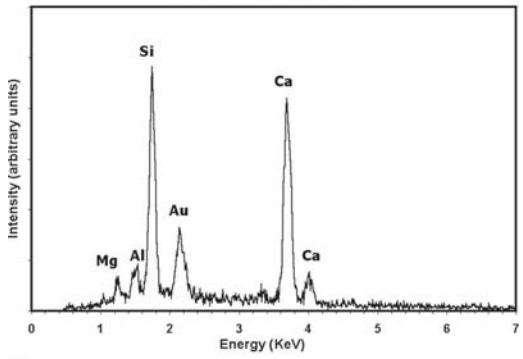

(b)

Fig. 6 (a) SEM image of the concrete surface adjoining the steel reinforcement in sample 3. (b) Its EDS spectrum

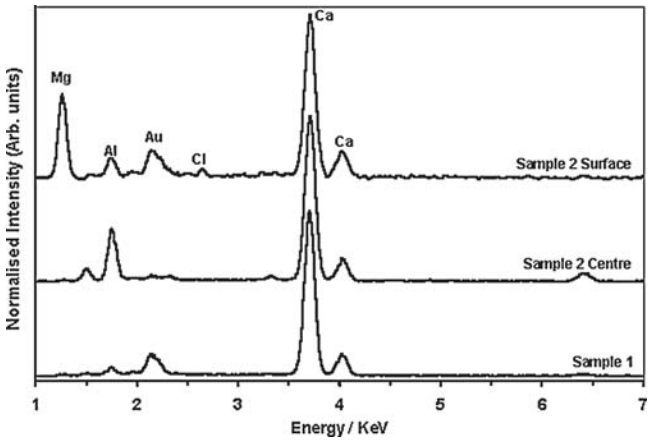

Fig. 7 EDS spectra from the surface and center of seawater-cured concrete (sample 2) compared with reference sample (sample 1), showing the presence of Mg and chloride on the surface of the seawater-cured sample

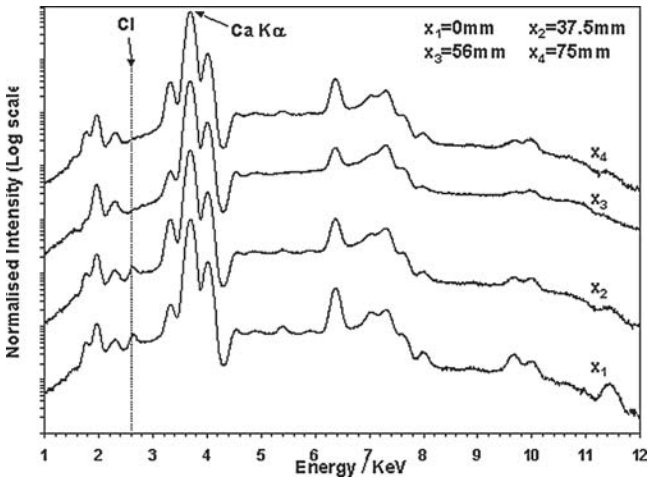

Fig. 8 PIXE analysis of the samples from different distances of the concrete block cured in seawater (sample 2, x = distance from surface)

distance of 40 mm is higher than that at the center. This behavior can be attributed to the diffusion of chloride during curing in seawater.

A similar analysis was carried out on sample 3 (i.e., a concrete well-cured in normal water and exposed to seawater for 7 days). The results of the analysis at different distances from the surface (Fig. 9) show no observable variation in chloride content as a function of distance.

The above results have been useful in understanding the diffusion processes in different concretes. The evaluation of D has been carried out using well-established diffusion models.

3.5 Modeling of Chloride Ingression in Concrete Cured in Sea Water

The process of the ingression of chloride from the surface into the concrete block has been modeled in one dimension, incorporating drift and diffusion mechanisms. The differential

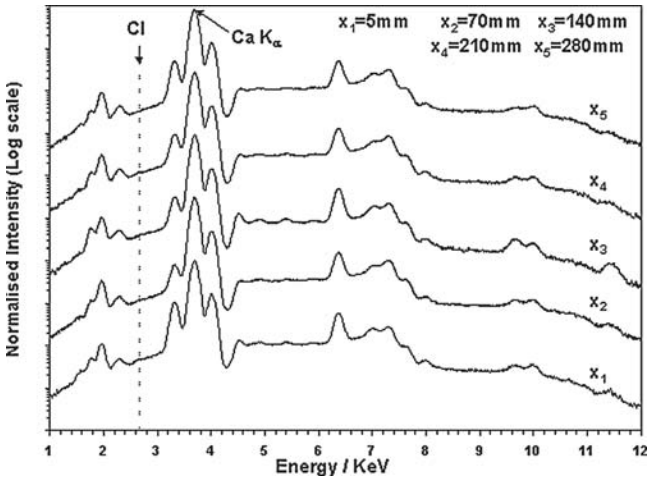

Fig. 9 PIXE analysis of the samples from concrete well cured in normal water, exposed to seawater for 7 days (sample 3, x = distance from surface)

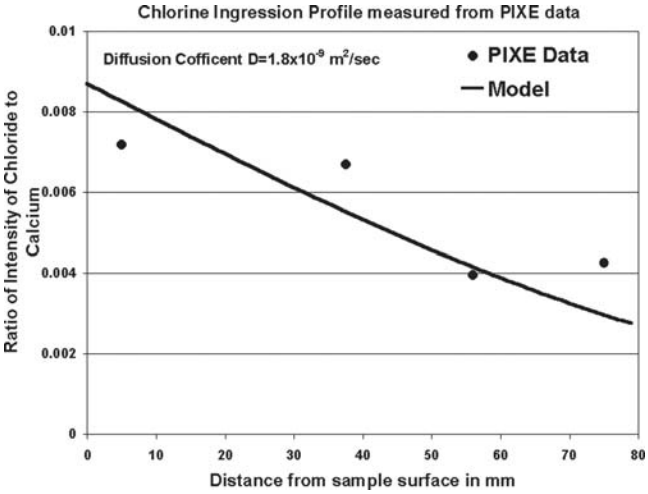

Fig. 10 Chloride profile obtained by a curve fitting the ratio of the intensity of chloride to Ca in concrete cured in seawater (sample 2), measured using PIXE

equation describing the change in chloride concentration (C) as a function of time (t) is given by:

$$\frac{\partial C}{\partial t} = D\frac{\partial^2 C}{\partial x^2} + V\frac{\partial C}{\partial x}$$

where x is the depth measured in meters from the surface, D is the diffusion coefficient (m^2/s) of chloride in concrete, and V is the drift velocity (m/s).

The solution for C as a function of position (x) and time (t) is given by:

$$C(x,t) - C_b = \frac{C(0,0) - C_b}{2}\left(Erfc\left[\frac{x - vt}{2\sqrt{Dt}}\right] + e^{\frac{vx}{D}}Erfc\left[\frac{x + vt}{2\sqrt{Dt}}\right]\right)$$

where, C (0, 0) is the concentration of chloride at the surface at $t = 0$, C_b is the base concentration of chloride in the concrete, and *Erfc* is the usual complementary error function.

The curve fitting the chloride concentration profile obtained experimentally allows D to be evaluated. It is then possible to quantify the chloride concentration at different distances and times. It is then possible to compare the computed values of chloride concentration for long service life against the specification limit. Thus, the extent of the penetration of chloride into the concrete can be estimated.

D was evaluated using the above equation and the semi-quantitative data obtained by PIXE analysis. The ratio of the intensities of chloride to calcium has been taken as an index of chloride content. The variation in this ratio as a function of depth from the surface is shown in Fig. 10. The diffusion coefficient obtained by the curve fitting the PIXE data from sample 2 was ~1.8×10^{-9} m^2/s. The value of D is higher than the values reported in the literature, which typically range from ~10^{-11} to 10^{-13} m^2/s (Ref 14-16). The diffusion kinetics of chloride in the seawater cured concrete appears to be two orders of magnitude higher compared with those of the cured concretes reported in the literature. This is attributed to the higher chloride ingression as a consequence of the higher amount of unreacted water and pores available for the diffusion of chloride ions during the curing process.

3.6 Prediction of Long-Term Diffusion Behavior of Chloride

Methods to predict the long-term concentration profile of chloride as a function of distance and time due to diffusion are presented. This methodology has been illustrated with a case study that required the prediction of chloride content as a function of distance and time, in a situation where structural concrete is built over seawater exposed (for 7 days) concrete. The build up of concrete layers is shown schematically in Fig. 11. It is expected that the concentration gradient would lead to the slow diffusion of chloride from the seawater exposed concrete to the structural concrete above. This would result in an increase in the chloride concentration of the structural concrete during its service life. The kinetics of this diffusion process is dictated by the diffusion coefficient. One method of retarding chloride transport into the structural concrete is to have an intermediate barrier of fly ash-containing concrete, which has a higher resistance to chloride diffusion. The extent to which chloride can diffuse from the surface of the seawater-exposed concrete to the surface of the barrier, consisting of 100 mm concrete packed with 28% fly ash, has been evaluated in this study using a simple diffusion model. The purpose of this study is twofold: to evaluate the chloride concentration at a distance of 100 mm in concrete with 28% fly ash after a time period of about 40 years, if the initial concentration C_0 of chloride at time $t = 0$ is known; and to evaluate the time it takes for the chloride concentration to exceed the safe limit of 0.6 kg/m^3 (Indian Standards [IS] 456–2000 specification) at a distance of 100 mm.

Figure 11 shows the chloride concentration profile at $t = 0$ as evaluated by experiments (Ref 11), the chloride distribution coefficient in different concrete, and the schematic of chloride redistribution across the concrete structure during the service life. The surface concentration C_s at $t = 0$ is equal to the seawater chloride content (i.e., 20,000 ppm).

The redistribution of chloride in the structure is governed by:

$$J = -D\left(\frac{\partial C}{\partial x}\right)_{at\ (x,t)}$$

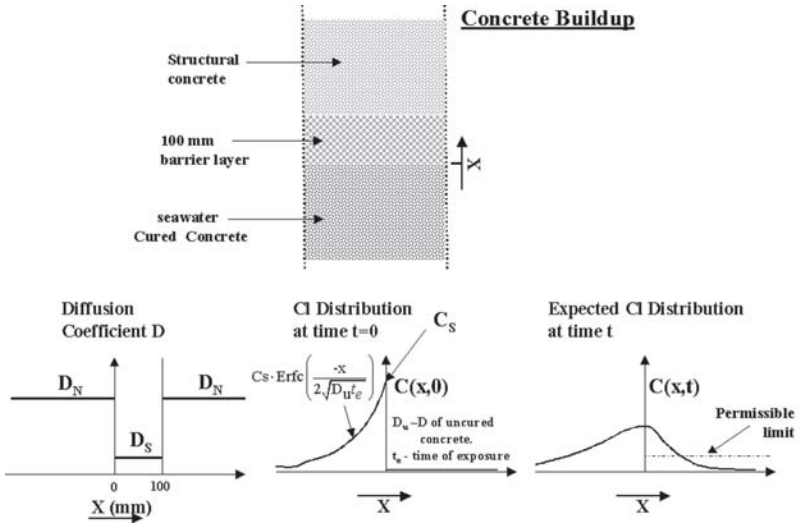

Fig. 11 Schematic of the case study of structural concrete built over seawater-exposed concrete with an intermediate barrier layer. D_N, diffusion coefficient of chloride in concrete; D_S, diffusion coefficient of chloride in concrete with fly ash

$$\frac{\partial C}{\partial t} = D\left(\frac{\partial^2 C}{\partial x^2}\right)_{at\ (x,t)}$$

Analytical solutions have been obtained using appropriate boundary conditions. Standard analytical solutions for problems, such as the finite source, or a constant concentration of semi-infinite thickness/finite thickness, are available. However, such a simplified analytical solution does not exist for the present problem of varying the diffusion coefficients across the structure using an initial Erfc distribution for the concentration. The problem has been simplified so that an analytical solution can be used to assess the redistribution behavior. The initial Erfc distribution is replaced by an equivalent rectangular distribution such that the net amount of chloride (i.e., the area under the rectangle/Erfc distribution) is the same. Also, the diffusion coefficient is constant throughout the concrete structure.

The solution for C as a function of height (x) and time (t) is then given by:

$$C(x, t) - C_b = (C_s - C_b) \cdot \left[-Erf\left(\frac{x}{2\sqrt{Dt}}\right) + Erf\left(\frac{x + 2h}{2\sqrt{Dt}}\right) \right]$$

where C_s is the initial surface concentration at $t = 0$ in the sea water-exposed concrete, C_b is the chloride concentration in the structural concrete (0.002%), h is the equivalent distance of the rectangular distribution, and Erf is the error function.

Based on the time of exposure of the concrete to seawater, the net amount of chloride ingression has been estimated. The initial distribution was taken as 2 wt.% (corresponding to the chloride content in seawater) and the effective distance (h) for the rectangular distribution was estimated at 37 mm. These values were used for determining C at various distances and times.

Figure 12(a) and (b) show the variation of chloride concentration as a function of time at $x = 100$ mm, and as a function of x for $t = 40$ years, respectively. The nature and type of chloride distribution in concrete with and without fly ash additions have been compared. The diffusion coefficients were taken from the literature (Ref 14-16) based on an analysis of well-cured (normal water) concrete structures that had been continuously exposed to seawater for several years.

The diffusion coefficient values from various sources are listed below:

- From Ref. 14: $D = 1.72 \times 10^{-13}$ m^2/s
- From Ref. 15: D without fly ash $= 8.70 \times 10^{-12}$ m^2/s
- D with fly ash $= 5.90 \times 10^{-13}$ m^2/s
- From Ref. 16: D without fly ash $= 1.49 \times 10^{-12}$ m^2/s
- D with fly ash $= 5.10 \times 10^{-13}$ m^2/s

It is seen from the available literature that the diffusion coefficient for chloride in concrete is substantially reduced by the addition of approximately 28% fly ash. Comparing the chloride profile with the allowable limit of 0.026 wt.% revealed that the chloride concentration at 100 mm and 40 years does not exceed the allowable limit.

Another method to confirm the above result was to evaluate the distance at which the two levels would be equal after 40 years. This analysis showed (Fig. 12b) that above a distance of about 80 mm, the concentration of chloride would be below the permissible limit. Hence, the thickness of fly ash (~100 mm) is more than adequate to prevent the ingress of chloride into the structural concrete.

4. Discussion

The strength, dimensional stability, and durability of concrete depend crucially on its microstructure. However, it has been difficult to arrive at a unified understanding of the influence of microstructure on the properties of concrete. The reasons are as follows: heterogeneous and complex microstructure; the presence of a large number of constituents; the presence of strong signatures of the regional diversities in the microstructure, making a unique description difficult; and the dependence of the structure of concrete on local humidity, temperature, and time, unlike other engineering materials, where the structure is an inherent characteristic of the material (Ref 12).

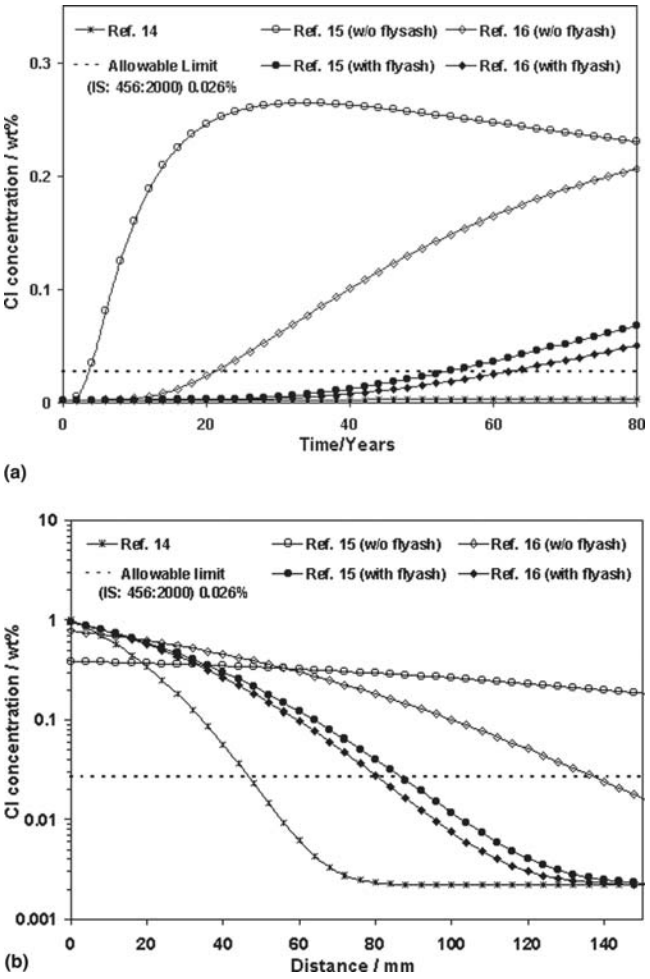

Fig. 12 Concentration profile of chloride as a function of (a) time at a distance of 100 mm of concrete with 28% fly ash and (b) distance for a time of 40 years

Despite these limitations, broad empirical knowledge of the structure and its influence on the properties of concrete has been established (Ref 12). The structure of concrete, at the first level of description, is considered as an inhomogeneous dispersion of four constituents: aggregate particles of different minerals consisting of different shapes and sizes; the binding medium of hydrated cement paste; the interface (~2–5 μm) between cement and the aggregates; and the system of voids, pores, and microcracks. The physical properties, like the size, shape, and distribution of the aggregate in the concrete, determine the unit weight, elastic modulus, and dimensional stability of concrete. The second major component of concrete, namely, the hydrated cement paste composed of solid particles of C-S-H gel, $Ca(0H)_2$, ettringite and its byproducts, and pores, is a dynamically evolving system. The formation of these compounds is understood by the "hydration" process of cement powder obtained by pulverizing cement clinker with gypsum (composed of clinker oxide compounds of Ca, Si, Al, and Fe such as tricalcium silicate, dicalcium silicate, tricalcium aluminate/ferrite, and calcium sulfate). The water-to-cement ratio, the type, size, amount, and distribution of "hydration products," including solids and voids/cracks in the cement, dictates the strength, dimensional stability, and durability of the concrete. The third constituent, namely, the interface, is a transition zone between the cement paste and the aggregate, and is the weakest link in the concrete. The nature of this zone combined with the system of pores, voids, and cracks decide the quality of the concrete. The results of the current study are discussed with respect to the microstructural, microchemical, and diffusion characteristics, based on the above description of the structure of concrete.

4.1 Microstructural and Microchemical Characteristics

The important microstructural and microchemical features studied in the three different types of concrete are summarized below:

- Identification of the constituents.
- Comparison of the quality of the surface between concrete cured in seawater and that cured in normal water.
- Distribution of chloride between the constituents of concrete showed preferential absorption in the cement phase.

Although there were differences between the two types of concrete at the visual level, at the microscopic level each had a similar microstructure with respect to the major constituents (i.e., aggregate, cement, interface, and the void/pore system). The aggregate consisted of solid mineral particles and gravel particles of various sizes. The particles were found to be rich in Si, Fe, and Ti, suggesting the presence of oxide minerals. However, the size distribution was nonuniform and heterogeneous. The matrix, namely, the hydrated cement paste, exhibited a heterogeneous structure of hydration products and pores. The nonuniform distribution of pore density is expected to introduce significant variations in the density of the concrete.

Apart from the above general observations, the concrete blocks cured in seawater showed distinct surface features with respect to surface roughness and color. No visible difference was observed in the pore density. The greenish-gray elongated features on the surface consisting of porous regions with faceted Ca-rich compounds and needle-like regions of Mg-rich compounds have possibly formed through salt deposition from the seawater.

The interfaces in samples 1 and 2 were observed to have the following features compared with the hydrated cement paste: larger size of hydration products; and higher porosity. The differences in the geometry of hydration products and the kinetics of hydration (Ref 17) in the interface, or transition zone, are attributed to the high water-to-cement ratio in the early stage of hydration. This is due to "bleeding" (i.e., the accumulation of more water around the interface of coarse particles of the aggregate than the finer particles). It is well known that the strength of the IFT zone depends on the volume and size of the voids present. The higher density of the pores and the size of the hydration products in the interface would result in poor adhesion between the cement and aggregate phase, making this zone the weakest link in the concrete structure.

The preferential absorption of chloride in the cement of the concrete is understood in terms of the higher permeability of water through the cement due to its porosity, in preference to the aggregate. The PIXE results for sample 3 show the absence of chloride at distances away from the surface, suggesting that the ingress of seawater through the pore system of this concrete could not proceed due to the nonavailability of a well-connected pore system. The absence of chloride in cement in contact with reinforced steel, 280 mm below the seawater-

exposed surface, is also in agreement with the above observation.

The microstructural and microchemical heterogeneities reported in the current study are fingerprints of the degree of hydration, which in turn depends on the ratio of water to cement. At the microscopic level, the localized water-to-cement ratio varies from one region to another, thereby introducing vast heterogeneities in the nature and distribution of hydration products.

4.2 Influence of Microstructure on Diffusion Characteristics of Chloride

The useful life of reinforced concrete structures is dictated by the kinetics of chlorination. Chloride adsorption-reaction and diffusion processes, in addition to desorption, in a dynamically evolving cement-pore system are complex. All microscopic constituents discussed above influence, to varying degrees, the ingress of chloride in concrete. The factors that dictate the chloride ingress in concrete, in order of importance are: the degree of connected pores in the cement of the pore/void system; the amount, composition, and mineralogical structure of the constituents in cement, which dictate the diffusion coefficient of chloride in cement; the size distribution of the aggregate, which plays a minor role because it indirectly determines chloride diffusion by controlling the extent of bleeding; and the interface zone, for similar reasons (Ref 18). The inferences drawn in the current study with respect to chloride ingress in the different concrete types are:

- Significant chloride ingression is observed only in concrete cured in seawater and not in concrete cured in normal water (i.e., concrete subsequently exposed to seawater).
- The diffusion coefficient of chloride in the seawater-cured concrete is two to three orders of magnitude higher than values in the literature (Ref 12-14).
- Calculations have shown that the presence of an intermediate 100 mm layer of concrete with 28% fly ash slows down chloride ingress between seawater-exposed concrete and structural concrete.

The first observation, namely, the significant ingress of chloride in concrete cured in seawater compared with concrete cured in normal water, can be understood as follows: in the initial stages, a large well-connected pore system is available, at least until the hydration of cement proceeds to a significant extent. The kinetics of the ingress of water being the same, chloride penetration measured in the seawater-cured concrete is apparently only a manifestation of the high chloride content in seawater (20,000 ppm), which is absent in normal water. This diffusion process, in principle, could have proceeded indefinitely, but for the simultaneous hydration process of the cement, which produces an impermeable, tighter pore system, thereby arresting further ingress.

Additionally, in the current study, chloride transport is assumed to be driven only by the diffusion phenomenon. However, it is expected that the hydration reactions in concrete would absorb a significant amount of chloride. This is expected to result in an apparently high value for the diffusion coefficient. The diffusion coefficients quoted in the literature are for well-cured concrete, subsequently exposed to seawater for several years. Hence, the higher value of D in seawater-cured concrete in the current study is as expected.

The chloride concentration has been predicted in structural concrete with an intervening barrier of concrete containing 28% fly ash. This has been done for an initial chloride concentration of 20,000 ppm and width (h), which is a limiting case for seawater exposure. This was done to determine the efficiency of the 100 mm layer of fly ash-containing concrete in preventing the flow of chloride ions into the adjacent structural concrete. The calculations show that the fly ash-concrete barrier effectively prevents the buildup of chloride for a period of up to 60 years. This is due to the very low diffusion coefficient of chloride in concrete with fly ash, which is achieved, in part, by the high silica content and the amorphous nature of fly ash.

5. Conclusions

The major conclusions of the current study are:

- The microstructural and microchemical features in concrete cured in normal water and seawater were studied using electron and ion optical spectroscopy techniques.
- The diffusion coefficient of chloride in seawater-cured concrete was evaluated by a curve fitting the results of the PIXE analysis. The high value of D is understood in terms of the chloride content in the poorly developed pore system of the wet concrete before the onset and progress of hydration reactions.
- The diffusion profiles of chloride for various times and distances have been evaluated using a simple diffusion model. A case study for the redistribution of chloride between concrete exposed to seawater and structural concrete with an intermediate barrier of fly ash, 100 mm thick, was presented.

References

1. V.G. Papadakis, M.N. Fardis, and C.G. Vayenas, Physiochemical Processes and Mathematical Modeling of Concrete Chlorination, *Chem. Eng. Sci.,* 1996, **51**(4), p 505-513
2. M.A. Climent, G. de Vera, J.F. López, E. Viqueira, and C. Andrade, A Test Method for Measuring Chloride Diffusion Coefficients Through Nonsaturated Concrete: Part I. The Instantaneous Plane Source Diffusion Case, *Cem. Concr. Res.,* 2002, **32**(7), p 1113-1123
3. P.F. McGrath and R.D. Hooton, Influence of Voltage on Chloride Diffusion Coefficients from Chloride Migration Tests, *Cem. Concr. Res.,* 1999, **26**(8), p 1239-1244
4. Z. Szantó, É. Svingor, M. Molnár, L. Palcsu, I. Futó, and Z. Szūcs, Diffusion of 3H, 99Tc, 125I, 36Cl and 85Sr in Granite and Concrete, *J. Radioanal. Nucl. Chem.,* 2002, **252**(1), p 133-138
5. O.M. Jensen, P.F. Hansen, A.M. Coats, and F.P. Glasser, Chloride Ingress in Cement Paste and Mortar, *Cem. Concr. Res.,* 1999, **29**(9), p 1497-1504
6. A.S. Clough and P.M. Jenneson, Ion Beam Analysis of Diffusion in Heterogeneous Materials, *Nucl. Instrum. Methods Phys. Res., Sect. B,* 1998, **139,** p 51-57
7. T. Zhang and O.E. Gjørv, Diffusion Behaviour of Chloride Ions in Concrete, *Cem. Concr. Res.,* 1996, **26**(6), p 907-917
8. R. Frey, T. Balogh, and G.L. Balázs, Kinetic Method to Analyse Chloride Diffusion in Various Concretes, *Cem. Concr. Res.,* 1994, **24**(5), p 863-873
9. T. Parthiban, R. Ravi, G.T. Parthiban, S. Srinivasan, K.R. Ramakrishnan, and M. Raghavan, Neural Network Analysis for Corrosion of Steel in Concrete, *Corros. Sci.,* 2005, **47**(5), p 1625-1642
10. P. Halamickova, R.J. Detwiler, D.P. Bentz, and E.J. Garboczi, Water Permeability and Chloride Ion Diffusion in Portland Cement Mortars: Relationship to Sand Content and Critical Pore Diameter, *Cem. Concr. Res.,* 1995, **25**(4), p 790-802
11. T. Karthikeyan, A. Dasgupta, P. Magudapathy, S. Saroja, M. Vijay-

alakshmi, K.G.M. Nair, K.P.N. Murthy, and B. Raj, "Microstructural and Microchemical Analysis on Mock Up and Site Concrete Samples from PFBR Using Analytical Techniques and Modeling of Chloride Diffusion," Report PFBR/01120/DN/1014, IGCAR, Kalpakkam, India, October 2005

12. P.J.M. Monteiro, Microstructure of Concrete, *Concrete: Structure, Properties and Materials,* 2nd ed., P. Kumar Mehta and Paulo J.M. Monteiro, Ed., Prentice Hall, 1993
13. K.L. Scrivener, Backscattered Electron Imaging of Cementitious Microstructures: Understanding and Quantification, *Cem. Concr. Comp.,* 2004, **26**(8), p 935-945
14. M.R. de Rooij and R.B. Polder, "What Diffusion Coefficient is Used for Cl Diffusion Modeling," presented at International Symposium on Advances in Concrete Through Science and Engineering, RILEM, March 21–26 (Evanston, IL), 2004, The Netherlands
15. M.D.A. Thomas and P.B. Bamforth, Modelling Chloride Diffusion in Concrete: Effect of Fly Ash and Slag, *Cem. Corros. Res.,* 1999, **29**(4), p 487-495
16. P. Sandberg, L. Tang, and A. Andersen, Recurrent Studies on Chloride Ingress in Uncracked Marine Concrete at Various Exposure Times and Elevations, *Cem. Concr. Res.,* 1998, **28**(10), p 1489-1503
17. K.-B. Park, T. Noguchi, and J. Plawsky, Modelling of Hydration Reactions Using Neural Networks to Predict the Average Properties of Cement Paste, *Cem. Concr. Res.,* 2005, **35**(9), p 1676-1684
18. C.C. Yang and S.W. Cho, Influence of Aggregate Content on the Migration Coefficient of Concrete Materials Using Electrochemical Method, *Mater. Chem. Phys.,* 2003, **80,** p 752-757